# A mathematical model for bleb expansion clarifies the role of TalA and actin dynamics in regulating bleb size and frequency

S.H. Dinuka S de Silva[1], Emily Movsumova[2], Jessica Reznik[2], Zully Santiago[2], Derrick Brazill[2], and Emmanuel Asante-Asamani[1,*]

[1]Department of Mathematics, Clarkson University, Potsdam, New York
[2]Department of Biological Sciences, Hunter College, New York

**Abstract**

Eukaryotic cells, such as cancer and immune cells, migrate using either pressure-driven blebs or actin polymerization driven pseudopods, with cells preferring to bleb in confined environments where high protrusion forces are required for movement. Blebbing involves a separation of the cell membrane from the cortex, via the detachment of membrane-to-cortex linker proteins. The detached membrane then expands and stabilizes into a spherical cap as a new cortex is formed beneath the protruded membrane while the old one is completely degraded. The role of linker proteins has mostly been associated with directing blebs to the leading edge of the cell, where linker enrichment is low, suggesting that cells devoid of linker proteins will bleb profusely. However, recent experiments suggest that knocking out the linker protein, TalA, in *Dictyostelium discoideum* cells decreases the cells ability to bleb. Additionally, little is known about how actin dynamics during bleb stabilization affect bleb size. In this work, we analyze the size and frequency of blebs in wild type and *talA* null *Dictyostelium discoideum* cells chemotaxing under a light and heavy agarose block. Our analysis reveals that *talA* null cells produce fewer and smaller blebs in confined environments, suggesting that linker proteins help the cell maintain intracellular pressure during blebbing. A mathematical model of bleb expansion developed and validated with our experimental data supports this hypothesis and identifies the polymerization to depolymerization rate of actin in the reforming cortex as a key regulator of bleb size and retraction dynamics in a myosin II independent manner.

Keywords: Blebbing, *Dictyostelium discoideum*, Cell Migration, Talin, Mathematical modeling, Chemotaxis
2020 Mathematics Subject Classification. Primary: 92C05, 92C17, 9205, 9210, 34D20

# Introduction

Blebs are spherical protrusions that are produced by cells as a mechanism for movement [14, 4, 11, 5], particularly as the confinement in the environment increases [16]. Bleb-based motility has been observed in many cell types including *Dictyostelium discoideum*, Zebrafish, and some cancer cells. *Dictyostelium* cells constrained under a block of agarose have been observed to move using blebbing [37, 2, 9]. Blebbing has also been implicated in regulating the migration of *Dictyostelium* cells within a multicellular mound [31]. Zebrafish premordial germ cells are able to migrate to the right location in the embryo using blebs [4, 22]. Additionally, metastasizing cancer cells undergoing single cell motility have been observed to move with blebs [17, 19, 15, 25], especially when drugs reduce the functionality of their actin polymerization machinery [12].

A hallmark of blebbing is the separation of the cell membrane from a local region of the cortex and its subsequent expansion into a spherical cap, powered by prevailing intracellular pressure [5, 21, 36]. This pressure is thought to be regulated by cortical tension, generated by myosin II-driven contraction of the acto-myosin cortex [21] or confinement forces within the cellular environment [16]. Indeed, myosin deletion cells fail to bleb whereas cells with reduced myosin contractility or confinement produce smaller blebs [27, 16]. As the membrane expands, a new cortex reforms beneath the protruded membrane and the old cortex (actin scar), at the original location of the detached membrane, completely degrades to stabilize the bleb [2, 3].

Prior to bleb expansion, the membrane is held to the cortex through membrane-cortex binding proteins (linker proteins). One such protein is talin whose orthologues in *Dictyostelium* are TalA and TalB [34, 20, 30]. TalA has been observed to cluster at the rear of chemotaxing *Dictyostelium Discoideum* cells [9, 34], where it prefers to bind to stretched actin filaments [32]. This rear clustering of linker proteins has been shown to direct blebs to the front of the cell, where very few TalA proteins accumulate. Quantification of experimental observations revealed that the area of the cell with the highest blebbing activity coincides with the area with lowest TalA enrichment [9]. In an under-agarose chemotaxis assay, *Dictyostelium* cells devoid of both TalA and TalB were observed to nucleate blebs more frequently (compared to wild type) at random locations around the cell boundary [9]. Taken together, these observations led to the conclusion that TalA enrichment

is inversely proportional to blebbing and that cells without TalA will bleb profusely.

In a recent study, TalB proteins were found to localize to the leading edge of chemotaxing *Dictyostelium* cells, where actin filaments are not as stretched as those found in the posterior of the cell [32]. Phenotypic differences have been observed in single deletions of *talA* and *talB*. For example, *talA* null cells are able to develop normally, however *talB* nulls arrest at the mound stage and cannot form tips [33]. On the other hand, *talA* null cells are defective in cytokinesis and forming adhesions with the substrate [20]. The distinct localization of these proteins coupled with their phenotypic differences suggests that the two proteins could have distinct roles in regulating blebbing. Additionally, the evidence provided to support the conclusion from [9] that *talA*/*talB* null cells bleb more profusely was more qualitative than quantitative. Taken together, it is unclear whether the observation of more frequent blebbing in the double talin mutant in [9] will be observed in a single deletion of TalA. Additionally, whereas blebbing is well known to involve a reformation of a cortex beneath the protruded membrane, and a degradation of the old cortex, very little work has been done to investigate the role of actin dynamics in the regulation of bleb size.

Our work examines the role of TalA in regulating blebbing during confined chemotaxis. Contrary to the existing school of thought, we find that *talA* null *Dictyostelium* cells, chemotaxing towards cyclic AMP under agarose, generate significantly fewer blebs than wild type cells. Using a combination of mathematical modeling and quantification of bleb size and cell area from experiments, we conclude that TalA helps to maintain the intracellular pressure necessary for bleb formation, so that in its absence the driving pressure to create blebs is reduced. Our model also helps to clarifies the role of actin dynamics in regulating bleb size.

# Materials and Methods

## Strain and culture conditions

The *Dictyostelium discoideum* cells were grown in shaking culture in HL5 medium with glucose (ForMedium), 100 IU/mL penicillin, and $100\mu g/mL$ streptomycin (Amresco) at 150 rpm at $22^0C$ or on 100mm culture plates. *talA* null (DBS0236180) cells were ordered from Dictybase.org and grown

on culture dishes. To generate the GFP expressing lines, both Ax2 (wildtype) and *talA* null lines were electroporated with the LifeAct-GFP plasmid, a generous gift from Dr. Chang-Hoon Choi [8], and selected with G418 (4-20 $\mu g/mL$). For details on transformation protocal, clone selection and confirmation of cell lines see [23]. The cell lines were sub-confluent in log phase ($1 \times 10^6 cells/mL$ to $4 \times 10^6 cells/mL$) from shaking prior to use for experiments [24].

## Cyclic-AMP (cAMP) under agarose assay

A preheated ($90^0 C, 1\ min$) number 1 German borosilicate sterile 2 well chambered coverglass slide (ThermoFisher) was loaded with $750 \mu L$ of melted 0.4% or 0.7% Omnipur agarose (EMD Millipore) laced with 1mg/mL of 70,000 MW Rhodamine B isothiocyanate-dextran (Sigma-Aldrich). Once solidified, half of the gel was removed from the well and the remaining portion was slid across to the middle of the chamber, creating two wells with one on each side of the gel. To create the cAMP gradient, $4 \mu M$ cAMP was loaded into one well and incubated for 40 minutes. $1 \times 10^5$ to $2 \times 10^5$ cells competent for cAMP chemotaxis were loaded into the other well and allowed to settle and crawl under the agarose for 30 minutes prior to imaging. See [24] for additional details.

## Live imaging and microscopy

All imaging data was acquired using a Leica DMI-4000B inverted microscope (Leica Microsystems Inc.) mounted on a TMC isolation platform (Technical Manufacturing Corporation) with a Yokogawa CSU 10 spinning disc head and Hamamatsu C9100-13 ImagEM EMCCD camera (Perkin Elmer) with diode lasers of 491 nm, 561nm, and 638 nm (Spectra Services Inc.) [104]. LifeAct-GFP and RITC-dextran were excited using the 491nm and 561nm lasers, respectively. Images were taken over the course of 30 seconds a 100x/1.44 oil immersion objective at maximum camera speed with exposure times of 0.800 seconds for GFP and 0.122 seconds for RITC channels, resulting in intervals of 1.66 seconds. Images were acquired using Volocity 5.3.3 (Perkin-Elmer) and processed in ImageJ. Cell motility structures with respect to their membrane positions were captured in real-time.

## Image processing

As cells crawled under a RITC-dextran laced agarose gel, actin structures were visualized by LifeAct-GFP while membrane position was visualized as a negative against the RITC background. The open access software ImageJ (https://imagej.nih.gov/ij/) was used. The raw data for each series, consisting of the membrane and cortex channels, were split and separated from each other and adjusted for optimal brightness and contrast using ImageJ. Once complete, the two channels (membrane and cortex) were merged together with the cortex in green and the membrane in red. The merged images were subsequently saved as an .avi file without any compression to be used for detection of blebs and calculation of bleb area. Note that, due to the confinement imposed by the agarose gel, cells flatten and adopt a 'pancake' shape with a near uniform cross sectional area. Thus our area measurements can be translated into cell/bleb volume by multiplying by the height of the gap between the agarose gel and the slide.

## Determining bleb frequency, bleb area and cell area

We analyzed the first 20 frames to determine the bleb frequency and area, since there were noticeable qualitative effects of the lasers on the cell behavior afterwards. To detect blebs, we looked for a clear separation of the membrane (from RITC-dextran channel) and a reformation of the cortex (from LifeAct-GFP channel). The number of blebs generated by a cell within the first 20 frames of observation was recorded as the frequency. The bleb area was calculated from the stabilized bleb, with a fully reformed bleb cortex and degraded actin scar (old cortex). The bleb area was calculated using our in-house Bleb Detection Algorithm [3]. This significantly cut down on the time required to process all cells. The algorithm takes as input a sequence of cell boundary coordinates (extracted from the cortex images) and returns the number and area of blebs detected within the time duration as well as the cell area. The number of blebs detected was compared with our manual counts. For any missed blebs, usually due to small size, the area was calculated manually using ImageJ. The polygonal tool in ImageJ was used to create an outline of the bleb. The resulting boundary was smoothed using the spline fit tool. Area measurements were obtained from the Analyze menu in ImageJ. A similar manual process was used to calculate the cell area.

## Statistical analysis

Bleb and cell area as well as bleb frequency measurements were obtained from two independent experiments for each confinement condition. Box plots were created to visualize the distribution of the bleb frequency and area. We pooled together the data from all trials under the same pressure condition, since they had similar distribution (see supplementary information). The Mann Whitney U test was used to check for significant differences between groups. Statistical analysis was done in R-studio.

## Mathematical model of bleb expansion

Our model for bleb expansion is based on the geometric assumption that cells adopt a 'pancake' shape under an agarose block with a height that decreases with the agarose concentration. Under this assumption, the cell shape is considered uniform along the z-axis, so that a two-dimensional image of the cell observed on any confocal plane is a good representation of its shape on other planes. Mechanically, we consider the cell to be a viscous fluid encased by a viscoelastic boundary comprising an elastic membrane, viscoelastic cortex and elastic linker proteins. Our modeling framework follows the approach used by Iglesias et al. to model cell deformation during micropipette aspiration [35] with significant modifications that adapt it to bleb formation.

### 1D Model for bleb expansion

We begin by creating a simple ode model that tracks the extension of the cell boundary along a radial line drawn from the center of the cell through a boundary point (See Figure 1A for an illustration). We model the cell boundary as a composite body comprising of an outer membrane supported by an inner cortex with linker proteins connecting the two structures. The membrane is a phospholipid bilayer, modeled as an elastic material with elastic stiffness $k_m$. The dense network of crosslinking and motor proteins holding branched actin filaments together in the cortex give it elastic and viscous properties, with the viscous behavior stemming from the dynamic renewal of actin filaments through polymerization and depolymerization [18, 10]. Thus, the cortex can be considered as a Kelvin-Voigt viscoelastic solid, with viscosity coefficient $\tau_c$ and elastic stiffness

$k_c$. Proteins linking the membrane to the cortex undergo continuous binding and unbinding, with a constant binding rate $k_{on}$ and a force dependent unbinding rate $k_{off}$. At any point along the boundary, the local density of bound linkers, $\rho_a(t)$ is assumed to induce an elastic resistance of $k_a\rho_a(t)$ to membrane separation with stiffness $k_a$ per linker protein.

During blebbing, the cell boundary extends due to motion of the cytosol, driven by intracellular fluid pressure. This motion is inhibited by the viscosities of the cytoplasm and cortex, stiffness of the cortex and membrane as well as the stiffness of linker proteins that bind the membrane to the cortex. Whereas the cell cortex in the local region where blebs form is mostly stationary, it degrades at the original cell boundary (actin scar) and is reformed at the new boundary created by the bleb (bleb boundary). This gives the bleb boundary time dependent mechanical properties as it transitions from a pure membrane to a membrane supported by a cortex. To capture the cells mechanical response to intracellular fluid pressure, we model the cell boundary and cytoplasm as a parallel arrangement of a damper, comprising of the viscous properties of the cytoplasm and cortex, and springs accounting for the elastic response of the membrane, cortex and linker proteins. The model is illustrated in (Fig. 1A, top).

Denoting the boundary displacement by $u$, our force balance equation becomes

$$F = (k_b + k_a\rho_a)u + (\tau_c + \tau_y)\dot{u}$$

which yields the following model for the boundary velocity

$$\frac{du}{dt} = \frac{F}{(\tau_c + \tau_y)} - \frac{(k_b + k_a\rho_a)}{(\tau_c + \tau_y)}u,$$

where $k_b = k_m + k_c$ is the composite stiffness of the boundary with contributions from the membrane and cortex. To model the dynamics of linker proteins, we follow the work in [1] and assume that linker proteins bind to the cortex at a rate proportional to the density of unbound linkers $\rho_0 - \rho_a$ and unbind from the cortex at a rate proportional to the boundary displacement, $u$. The final model for bleb expansion along a radial line becomes

$$\frac{du}{dt} = \frac{F}{(\tau_c + \tau_y)} - \frac{(k_b + k_a\rho_a)}{(\tau_c + \tau_y)}u. \tag{1}$$

$$\frac{d\rho_a}{dt} = k_{on}(\rho_0 - \rho_a) - k_{off}(u)\rho_a \tag{2}$$

where $k_{off}(u) = k^0_{off}e^{\beta k_a u\delta}$. Here, $k^0_{off}$ is the rate at which linker proteins detach at zero displacement, $\beta$ is the thermal energy and $\delta$ is the characteristic bond length. We note that whereas our model for the boundary displacement in Eqn. 1 is similar to the model in [35], it is distinct because it accounts for the resistance of linker proteins through the term $k_a\rho_a$ and couples the viscous element of the cytoplasm in parallel with the viscoelastic element of the cell boundary. The combination of Eqn. 1 and Eqn. 2 to describe bleb expansion is also unique to this work.

The applied force, $F$ during bleb expansion is a pressure gradient force, determined by the difference in fluid pressure between the cytoplasm (high pressure) and the small region of detached membrane at nucleation (low pressure). As the bleb expands, the fluid pressure in the blebbing region increases. The bleb continues to expand until the net pressure between the two regions is zero. A similar force has been used to study the role of cortical tension on bleb size by Tinevez et al. [28]. A more complete description of this force will be presented in our two dimensional model for blebbing. In 1D, we model it as an exponentially decreasing force $F(u) = F_0e^{-mu}$ with decay rate $m$ and initial pressure $F_0$.

As pointed out earlier, the cell boundary and local cytoplasm have dynamic mechanical properties in the region where blebs form. Initially, the separation of the membrane from the cortex creates a purely elastic boundary which expands under the force of pressurized cytosol, devoid of large proteins, organelles and macromolecules which may not have made it across the pores of an intact cortex [26]. As the cortex reforms beneath the protruded membrane and degrades at the actin scar (old location of the cortex), the bleb boundary becomes more viscoelastic (with the addition of actin and associated crosslinking proteins). The fluid within the bleb also becomes more viscous, since more organelles and larger proteins make their way across the degrading cortex and a new cytoskeleton forms. We model the time dependent boundary elasticity ($k_b$) and viscosity of

the cortex ($\tau_c$) and cytoplasm ($\tau_y$), as

$$
\begin{aligned}
\tau_y(t) &= \gamma\tau_y^0 + (1-\gamma)\tau_y^0(1-e^{-k_{as}^{off}t}) \\
\tau_c(t) &= \tau_c^0 \frac{k_{ab}^{on}(1-e^{-k_{ab}^{off}t})}{k_{ab}^{off}} \\
k_b(t) &= k_m + k_c \frac{k_{ab}^{on}(1-e^{-k_{ab}^{off}t})}{k_{ab}^{off}}
\end{aligned}
\tag{3}
$$

where $k_{as}^{off}$ is the disassembly rates of the actin scar (degrading cortex) and $k_{ab}^{on}$ and $k_{ab}^{off}$ are polymerization and depolymerization rates of the reforming cortex respectively. The parameter $\gamma$ is a measure of cortex permeability, which regulates the initial viscosity of the local cytoplasm (within the bleb) $\gamma\tau_y^0$ immediately the membrane detaches. Here, $\tau_y^0$ is the viscosity of the cell cytoplasm (or the resting viscosity of fluid within the bleb). These equations are derived from our recent model describing actin dynamics during bleb stabilization [2]. See Supplementary Information for more details on the derivation of Eqn. (3).

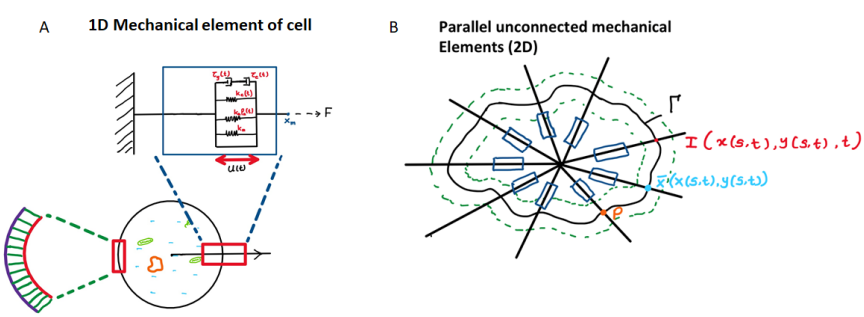


Figure 1: **Mechanical assumptions for mathematical model.** A) 1D mechanical element of the cell. B) 2D organization of 1D mechanical elements

**Bleb Initiation:** For a given pressure $F_0$ we first determined the boundary displacement and linker density for which the cell boundary and cytoplasmic resistance would balance out the driving pressure. We refer to these as the critical displacement and critical density, denoted by $u^0$ and $\rho_a^0$ respectively. Blebs are initiated by setting these critical values as the initial condition for our ode model (Eqn. (1) - Eqn. (3)). The critical displacement and density were obtained by solving

for the steady-states of Eqn. (1) and Eqn. (2) with constant mechanical parameters (set to their value before bleb nucleation). We then mimic the detachment of linker proteins by setting $\rho_a = 0$. Details on how the steady-state values of the model were calculated has been provided in the Supplementary Information.

## 2D model for bleb expansion

Whereas a 1D model of bleb expansion provides a system of ODEs which are relatively easy to analyze and simulate, it does not provide a full description of the driving pressure that generates blebs or the dynamics of linker proteins as the membrane peels away from the cortex. Using the 1D model as a foundation, we build a model of blebbing in two-dimensions (2D). Inspired by the work of Iglesias [35], we describe the mechanical response of the cell to applied intracellular pressure as equivalent to an array of unconnected 1D elements, illustrated in Figure 1B. We assume further that at each time $t$, the displacement vector $I(x, y, t) \in \mathbb{R}^2$, varies continuously along the cell boundary, with magnitude in the normal direction given by the 1D displacement $u(t)$. Here, $x = x(s, t), y = y(s, t)$ are the coordinates of the cell boundary $\Gamma(t) := \{(x(s, t), y(s, t)) : s \in [a, b]\}$. Similarly, we assume that the density of linker proteins, denoted by $= P(x, y, t)$, varies continuously along the cell boundary. In order to compute spatial derivatives of these quantities, we need them to be defined in a neighborhood around the cell boundary. Consequently, we extend $I$ and $P$ to be defined off the boundary by assuming that they are constant in the unit normal direction ($\hat{n}$) to the interface. With this assumption, we obtain the following 2D model for bleb expansion

$$\frac{\partial I}{\partial t} - \frac{\vec{\tau}.I}{|\vec{\tau}|^2}\frac{(k_b + k_a P)}{\tau_c + \tau_y}\frac{\partial I}{\partial s} = \frac{F_{drv}\hat{n}}{\tau_c + \tau_y} - \frac{\left(k_b + k_a P\right)}{\tau_c + \tau_y} I \tag{4}$$

$$\frac{\partial P}{\partial t} - \frac{\vec{\tau}.I}{|\vec{\tau}|^2}\frac{(k_b + k_a P)}{\tau_c + \tau_y}\frac{\partial P}{\partial s} = k_{on}[\rho_0 - P] - k_{off}(|I|)P \tag{5}$$

where

$$
\begin{aligned}
\tau_y(s,t) &= \tau_y^0(1 - X_{bleb}(s)) + [\gamma\tau_y^0 + (1-\gamma)\tau_y^0(1 - e^{-k_{as}^{off}t})]X_{bleb}(s) \\
\tau_c(s,t) &= \tau_c^0(1 - X_{bleb}(s)) + [\frac{\tau_c^0 k_{ab}^{on}(1 - e^{-k_{ab}^{off}t})}{a_0 k_{ab}^{off}}]X_{bleb}(s) \\
k_b(s,t) &= (k_m + k_c)(1 - X_{bleb}(s)) + \left[k_m + \frac{k_c k_{ab}^{on}(1 - e^{-k_{ab}^{off}t})}{a_0 k_{ab}^{off}}\right] X_{bleb}(s).
\end{aligned}
\tag{6}
$$

Here $\vec{\tau}$ is the tangent vector to a point on the interface, $F_{drv}$ as the driving pressure, $\tau_c(s,t), \tau_y(s,t)$ and $k_b(s,t)$ are 2D extensions of the time dependent mechanical parameters described in Eqn. (3). A full derivation of the model is presented in the supplementary information.

One of the limitations of our 1D model is the pressure term, which is quite phenomenological. We derive a more mechanistic model by setting $F_{drv}$ to be

$$
F_{drv} = P_{cell} - X_{bleb}P_{bleb} \tag{7}
$$

where $P_{cell}$ is the cytoplasmic pressure in the cell and $P_{bleb}$ is the pressure inside the bleb. Here $X_{bleb}$ is an indicator function for the region of the cell where a bleb forms. Recall from Laplace's Law that the pressure across a circular interface with curvature $\frac{1}{r}$ subject to boundary tension $\gamma$ is $\frac{2\gamma}{r}$. We extend this to non-circular interfaces as $2\gamma\kappa$, where $\kappa$ is the boundary curvature. Blebbing cells tend to preserve a constant cell volume[29]. To enforce this, we introduce a volume pressure term that decreases (increases) the cytoplasmic pressure if the cell volume increases (decreases). Additionally, we introduce a pressure term, $P_{start}$ to capture some excess intracellular pressure induced by say actomyosin contraction before bleb initiation. Thus, the cytoplasmic pressure $P_{cell}$ takes the form

$$
P_{cell} = P_{cell}^0 + k_{cell}\ln\left(\frac{A_0}{A}\right) + P_{start}. \tag{8}
$$

Here, $P_{cell}^0 = 2\gamma_{cell}\kappa_{cell}$ is the resting hydrostatic pressure of the cell with $\gamma_{cell}$ and $\kappa_{cell}$ as the boundary tension and curvature. The bulk modulus of the cytoplasm is denoted as $K_{cell}$ with $A_0, A$ as the initial and current cell area. Observe that we can use the cell cross sectional area instead of volume in the volume constraint term because of our initial geometric assumption. We

model the bleb pressure similarly as

$$P_{bleb} = 2\gamma_{bleb}\kappa_{bleb} \tag{9}$$

where $\gamma_{bleb}, \kappa_{bleb}$ represent the tension and curvature of the bleb boundary.

**Bleb Initiation:** Prior to bleb initiation, we assume a resting intracellular pressure $P^0_{cell}$ is balanced by the resistance of the viscoelastic boundary and linker proteins (with base line mechanical parameters). This sets the displacement vector $I$ and linker density $P$ to some critical value. To obtain these critical values, we assume there is initially no spatial variation in the boundary displacement $I$ and critical density $P$ around the cell. Thus, $\frac{\partial I}{\partial s} = \frac{\partial P}{\partial s} = 0$ in the 2D model. Assuming further that any initial boundary displacement occurs in the normal direction ($\hat{n}$), we can set $I = u\vec{n}$, which allows us to use the 1D critical displacement $u^0$ and linker density $\rho^0$ as initial conditions for the 2D model. To initiate blebs, we assume the cell generates an excess pressure $P_{start}$ which detaches linker proteins within some section of the boundary.

# EXPERIMENTAL RESULTS

We investigated the role of TalA in regulating blebbing by analyzing bleb characteristics (frequency and area) from wild type *Dictyostelium discoideum* cells (Ax2) and *talA* null cells, chemotaxing under an agarose block. See Fig. 2A for an illustration of the under-agarose setup used for experiments and Materials and Methods for a complete description of the assay. Cells were observed under low confinement (0.4% agarose) and high confinement (0.7% agarose) for a duration of 30 seconds each. A an example of blebbing in Ax2 and *talA* null cells is shown in Fig. 2(B,C). Notice the complete bleb cycle in Ax2 cells of membrane separation (5.85 secs), cortex reformation and accumulation of F-actin inside the bleb (7.80 secs) and complete degradation of the cortex at 17.55 secs, which is consistent with previous published work. A similar cycle can be observed in *talA* null cells. The total number of cells analyzed and the number of blebs produced by these cells are provided in Table 1. The data represents observations pooled from two independent experimental

trials. Bleb characteristics were measured after the cortex, visualized with LifeAct-GFP, had fully formed around the protruded membrane in both Ax2 and *talA* null cells.

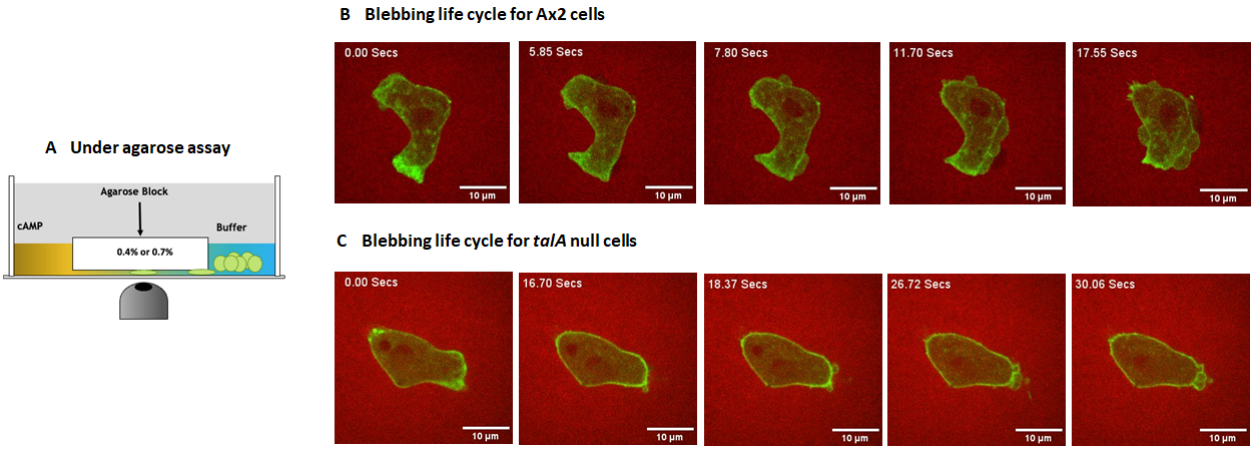


Figure 2: **Blebbing Ax2 and *talA* null cells** A) Illustration of underagarose assay used to collect data on blebbing chemotaxing cells. An illustration of b) wild type cell and c) *talA* null cell blebbing under 0.7% agarose. Factin is marked by LifeAct-GFP and the membrane is shown as a shadow against the agarose gel lased with RITC-dextran (red)

Table 1: **Summary of experimental data.** This table summarizes the cellular data analyzed. The "Total cells analyzed" reflects counts for all cells (in frame and not in contact with other cells) that were used. The "Total cells that blebbed" is the number of cells that had at least one bleb.

| | Ax-2 0.4% | *talA* null 0.4% | Ax-2 0.7% | *talA* null 0.7% |
|---|---|---|---|---|
| Total cells analyzed | 23 | 103 | 18 | 157 |
| Total cells that blebbed | 18 | 10 | 16 | 50 |
| Total number of blebs | 76 | 18 | 73 | 143 |

## *talA* null cells produce fewer blebs than wild type

We analyzed the proportion of wild type (Ax2) and *talA* null cells that produced blebs under low and high confinement. A total of 23 Ax2 cells were analyzed under low confinement conditions with 78% of them producing at least one bleb (Table 1). On the contrary, just under 10% of the *talA* null cells bleb. A similar pattern can be observed under high confinement. Whereas about 90% of Ax2 cells produce at least one bleb, just about 30% of *talA* null cells bleb. We compared the number of blebs produced per cell in Ax2 and *talA* null cells. As illustrated in Fig. 3A, *talA* null cells produce

fewer blebs than Ax2 under all confinement conditions. Whereas Ax2 cells produce a median of 4 blebs per cell, under low confinement, the median bleb frequency in *talA* null cells is zero under similar conditions. Both cells appear to increase their bleb frequency in response to confinement. Contrary to expected results, these data suggest that *talA* null cells bleb less frequently than wild type under any confinement condition, with a higher proportion of them blebbing in environments with higher confinement.

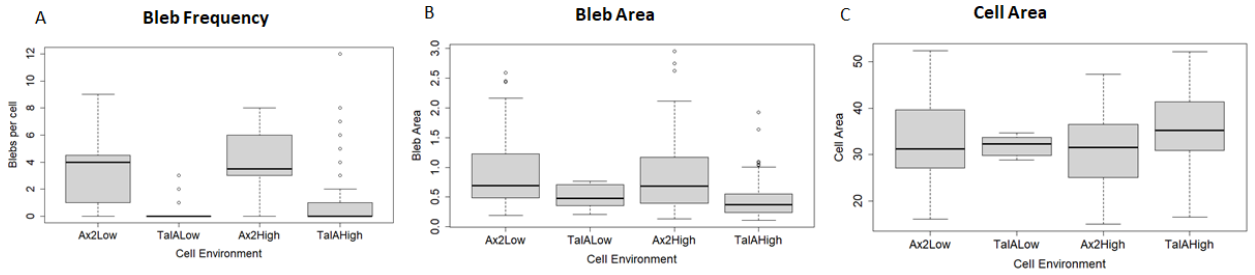


Figure 3: **Experimental data.** Data on a) frequency of blebs per cell b) bleb area c) Cell area for both wild type (Ax2) and mutant (*talA* null) cells shown in Table 1. Ax2High ( wild type under high confinement), Ax2Low (wild type under low confinement), TalAHigh (*talA* null under high confinement) and TalALow (*talA* null under low confinement).

## *talA* null cells have smaller blebs and larger cell surface area than wild type

Blebs are driven by intracellular pressure which is regulated by actomyosin contractility of the cortex. Tinevez et al. have identified the existence of a critical cortical tension (i.e intracellular pressure) above which cells form blebs [27]. Since *talA* null cells rarely bleb, we reasoned that this could result from a low intracellular pressure. Bleb size correlates with intracellular pressure [26, 16], therefore it can act as a gauge for the amount of pressure in the cell [6]. Thus, we tested our hypothesis by measuring the size of blebs produced by *talA* null cells and compared it to bleb size of Ax2 cells. Bleb size is characterized as the cross sectional area of the visible bleb from our microscopy images. See Materials and Methods for details on how area measurements were taken.

The distribution of bleb area measurements is shown in Figure 3B. Notice that, *talA* null cells have smaller bleb area than wild type under all confinement conditions. The decrease in bleb size under high confinement was found to be statistically significant (pvalue $< 0.01$) whereas that for

low confinement was not (pvalue=0.08). Bleb size remains fairly constant for each cell line under different levels of confinement (p-value=0.63: Ax2, p-value=0.17: *talA* null). These findings suggest that *talA* null cells have lower intracellular pressure, with a greater reduction in pressure observed in environments with high confinement.

Next we ask how TalA could regulate intracellular pressure. Fluid pressure in the cell is inversely proportional to the surface area to volume ratio of the cell. *Dictyostelium* cells are known to maintain an almost constant fluid volume during migration [7], therefore changes in the surface area of the cell could reduce the intracellular pressure. We sought to determine whether *talA* null cells have increased surface area, which would explain the low intracellular pressure. To achieve this, we compared cross sectional area (2 dimensional) of *talA* null cells to Ax2 under different confinement conditions. Our results, presented in (Figure 3C) show that *talA* null cells have a larger cross sectional area than Ax2 under high confinement (p-value$< 0.01$). No significant difference in cell area was observed under low confinement. This data supports our hypothesis that the reduced pressure in *talA* null cells is driven by an increase in the surface area of the cell.

# THEORETICAL RESULTS

The question that remains is why a loss of TalA would result in an increase in the surface area of the cell? We reasoned that knocking out *talA* leaves the membrane weakly bound to the cortex by TalB. This weaker membrane-cortex attachment could result in a uniform extension of the membrane away from the cortex when the cell is pressurized, creating an initial pressure relief that limits the prevailing pressure for blebbing. A similar observation was made by Tsujioka et al.[34] where *Dictyostelium* cells devoid of TalA left membrane tails in the cell posterior.

In what follows, we develop a mathematical model of bleb expansion to directly test the hypothesis that decreasing the strength of linker proteins lowers the prevailing pressure for bleb expansion by uniformly pushing the membrane from the cortex. The model is also used to investigate the influence of cortex reformation and degradation dynamics in regulating bleb size. We model bleb expansion in two stages. First, a one dimension model (1D) is developed (see Eqn. (1)-Eqn. (3) in Materials and Methods) and used as the foundation for a more relevant two dimensional (2D)

model (see Eqn. (4)-Eqn. (9) in Materials and Methods). We validate our mathematical models by exploring their ability to replicate known effects of cell mechanical parameters on bleb size. Our recent experimental data on the dynamics of bleb formation suggests that blebs reach maximum size within the first 6-10 seconds after membrane separation and equilibrate by 25 seconds [2]. Therefore, we simulate our models (first 1D and then 2D) for 10-25 seconds. All model parameters used in the simulation are presented in Table 2, with their corresponding references. Since the 1D model is the foundation for our 2D model, we validate that first before validating the full 2D model. The 1D and 2D models are solved using MATLAB's ode45 and ode113 receptively. Details of our procedure for bleb initiation is presented in the Materials and Methods. The Supplementary Information provides additional details on the numerical discretization of the 2D model.

## Effect of cell viscoelastic properties on bleb size

When the membrane first detaches from the cortex it expands under the force of flowing cytosol, driven by intracellular pressure and resisted only by its stiffness, $k_m$ and initial fluid viscosity $\tau_y$. As the cortex begins to reform beneath the membrane and degrade at the old location of the cortex, the boundary resistance increases and slows down bleb expansion. It is well known that bleb size increases with increasing intracellular pressure (or environmental confinement) and decreases as the viscoelastic properties of the cortex and membrane increases [16, 26, 37]. It has also being observed experimentally that as actin reforms beneath the protruded membrane, the bleb boundary undergoes a partial retraction [2]. We sought to test our model's ability to capture these known trends by varying our model parameters. The size of blebs in the 1D model is taken to be the displacement $u$ of the cell boundary at a fixed point. We allowed the cortex-free bleb to expand for 2 seconds before beginning cortex reformation, as was determined from experimental data in our previous study [2].

Our results in Fig. 4 and Fig. 5 both demonstrate the expected dynamics of a bleb. That is, a rapid expansion within the first 2 seconds and slower expansion or retraction to an equilibrium size after cortex reformation is initiated. We varied the resting intracellular pressure $F_0$ and membrane stiffness $k_m$, cortex stiffness $k_c$ and baseline cortex viscosity $\tau_c^0$ by scaling them from 0.1 to 10 times

| Parameter | Description | Value | References |
|---|---|---|---|
| $F_0$ | Cellular pressure | $0.08\ nN/(\mu m)^2$ | [29] |
| $m$ | Rate at which driving pressure decreases | 0.1 | This work |
| $r$ | Radius of the cell | $5\ \mu m$ | This work |
| $\tau_c^0$ | Viscosity coefficient of the full cortex | $0.064\ nNs/(\mu m)^3$ | [35] |
| $a_{rest}$ | Equilibrium actin density | $k_a^{on}/k_a^{off}$ | [2] |
| $k_a^{on}$ | Actin polymerization rate | 0.7602 | [2] |
| $k_a^{off}$ | Actin depolymerization rate | 0.4344 | [2] |
| $k_{as}^{off}$ | Actin depolymerization rate at actin scar | 0.0120 | [2] |
| $\tau_y^0$ | Viscosity coefficient of cytoplasm | $6.09\ nNs/(\mu m)^3$ | [35] |
| $k_{cell}$ | Bulk modulus of the cell body | $0.225\ nN/(\mu m)^2$ | [29] |
| $k_c^0$ | Spring constant for the cortex | $0.098\ nN/(\mu m)^3$ | [35] |
| $\gamma$ | Ratio of membrane stiffness to cortical stiffness | 1/25 | [26] |
| $k_a$ | Strength of single linker protein | $10^{-1}\ nN/(\mu m)$ | [1] |
| $\rho_0$ | Total available density of linker protein | $10^2\ (\mu m)^{-2}$ | [1] |
| $k_{on}$ | Binding rate of linker protein | $10^4\ (s)^{-1}$ | [1] |
| $k_{off}^0$ | Detaching rate of linker protein | $10\ (s)^{-1}$ | [1] |
| $k_m$ | Spring constant for membrane | $0.00392\ nN/(\mu m)^3$ | Estimate using [35] |
| $\beta$ | 1/Thermal energy $(k_BT)^{-1}$, $k_B$ is Boltzmann constant and $T$ is thermodynamics temperature | $\frac{10^6}{4.1}\ ((nN)(um))^{-1}$ | [1] |
| $\delta$ | characteristic bond length | $10^{-3}(\mu m)$ | [1] |
| $k$ | Elastic constant of spring like linkers | $10^{-1}\ nN/(\mu m)$ | [1] |
| $\gamma_m$ | Membrane tension | $0.032\ nN/(\mu m)$ | Estimate using [26] |
| $\gamma_c$ | Cortical tension | $0.2\ nN/(\mu m)$ | Estimate using [26] |

Table 2: Parameter values for simulating the bleb expansion models

their basal values given in Table 2. Observe from Fig. 4A that bleb size increases with intracellular pressure. Similarly, as membrane elastic stiffness decreases, the bleb expands faster to a higher maximum size and then retracts to a larger equilibrium size (Fig. 4B). As the cortex stiffness decreases, blebs expand faster and settle down to a larger equilibrium size (Fig. 4C). Interestingly, there appears to be two separate bleb expansion regimes regulated by cortical stiffness, one in which blebs retract after reaching their maximum size and the other where blebs do not retract, but expand gradually to their equilibrium size. Surprisingly, varying cortex viscosity, does not alter equilibrium bleb size, rather it appears to regulate the speed of expansion with less a viscous cortex

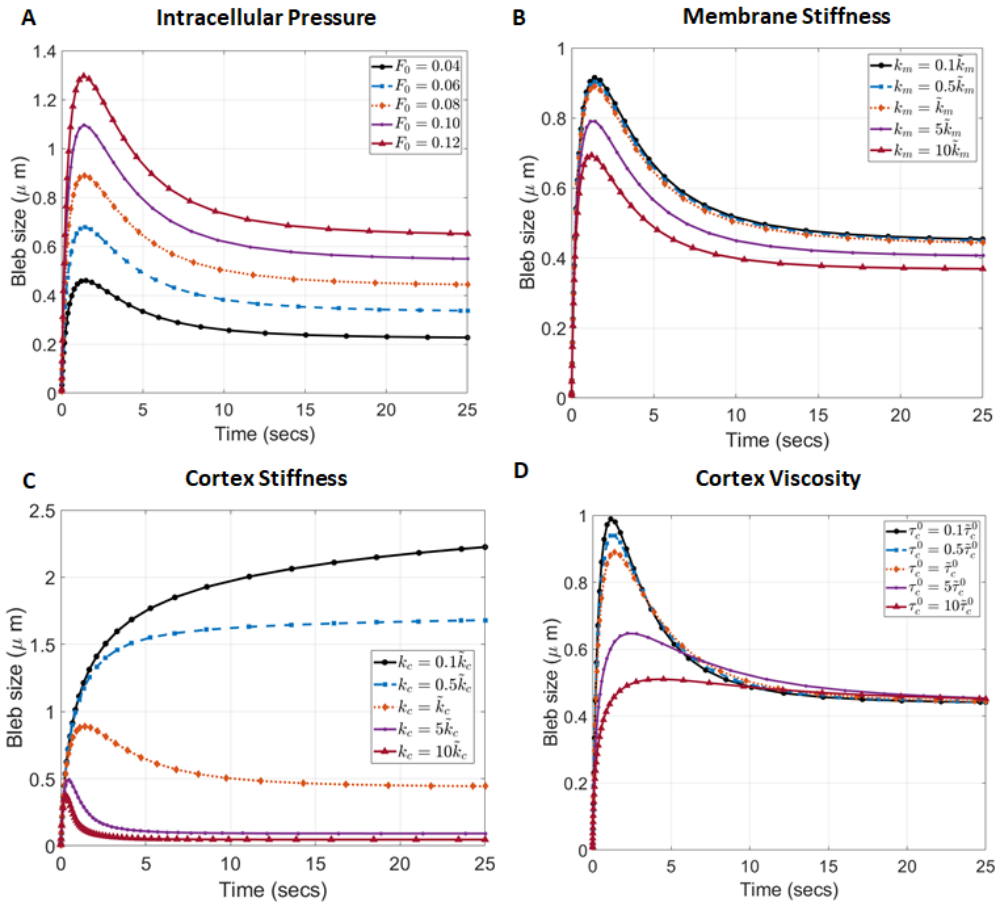


Figure 4: **Influence of cell mechanical properties on bleb size.** Effect of A) Intracellular pressure B) membrane stiffness, C) cortex stiffness and D) cortex viscosity. Bleb size is measured as the strain of the cell boundary at a single point. $\tilde{r}$ is the baseline value of parameter $r$ reported in Table 2.

leading to a larger maximal bleb size (Fig. 4D). Together, these results support the known behavior of expanding blebs and serve as a semi-quantitative validation of our 1D model.

## Effect of actin dynamics, cortex permeability and cytoplasmic viscosity on bleb size

We found it interesting that the equilibrium bleb size does not seem to depend on the cortex viscosity but depends on membrane and cortex stiffness as well as intracellular pressure. Curious about whether this is supported theoretically and also to identify other model parameters influencing the equilibrium bleb size, we analyzed the equilibrium solutions of the 1D model (Eqn. (1)) with $\rho_a = 0$

and time dependent parameters described in Eqn. (3). Note that by setting $\rho_a = 0$, we remove linker proteins from equilibrium analysis since they are detached when the membrane separates from the cortex. In order to perform equilibrium analysis, we converted the 1D model (Eqn. (1)), with $\rho_a = 0$, to an autonomous differential equation by writing separate rate equations for all time dependent parameters described in Eqn. (3) .This resulted in the following system of autonomous equations

$$\frac{du}{dt} = \frac{F(u)}{\tau_c + \tau_y} - \frac{k_b u}{\tau_c + \tau_y} \tag{10}$$

$$\frac{dk_b}{dt} = \frac{k_c}{a_0}(k_{ab}^{on} - k_{ab}^{off} a_{bleb}) \tag{11}$$

$$\frac{d\tau_c}{dt} = \frac{\tau_c^0}{a_0}(k_{ab}^{on} - k_{ab}^{off} a_{bleb}) \tag{12}$$

$$\frac{d\tau_y}{dt} = (1-\gamma)\tau_y^0 k_{as}^{off} a_{scar} \tag{13}$$

$$\frac{da_{bleb}}{dt} = k_{ab}^{on} - k_{ab}^{off} a_{bleb}. \tag{14}$$

$$\frac{da_{scar}}{dt} = -k_{as}^{off} a_{scar}. \tag{15}$$

A detailed formulation of the above autonomous system is given in the Supplementary Information. From Eqn. (15) and Eqn. (14) it is obvious that the equilibrium concentrations of actin in the actin scar and bleb cortex are, $a_{scar}^* = 0$ and $a_{bleb}^* = \frac{k_{ab}^{on}}{k_{ab}^{off}}$, respectively. The equilibrium cortex and cytoplasmic viscosity as well as boundary stiffness can be obtained directly from Eqn. (3) as $k_b^* = k_m + \frac{k_c}{a_0}\frac{k_{ab}^{on}}{k_{ab}^{off}}$, $\tau_c^* = \frac{\tau_c^0}{a_0}\frac{k_{ab}^{on}}{k_{ab}^{off}}$ and $\tau_y^* = \tau_y^0$, since Eqn. (11), Eqn. (13) and Eqn. (12) yield no additional conditions for equilibrium. Thus, we have the following condition for equilibrium bleb size

$$F_0 e^{-mu^*} - \frac{k_c k_{ab}^{on}}{a_0 k_{ab}^{off}} u^* = k_m. \tag{16}$$

which confirms the dependence of bleb size ($u^*$) on initial intracellular pressure, $F_0$, cortex stiffness $k_c$ and membrane stiffness $k_m$, observed from our model simulations. Additionally, the condition (Eqn. (16)) points to a dependence of equilibrium bleb size on actin reformation dynamics through

the ratio of actin polymerization and depolymerization rate $\frac{k_{ab}^{on}}{k_{ab}^{off}}$. However, the degradation rate of the actin scar (old cortex), cytoplasmic viscosity and cortex permeability have no effect.

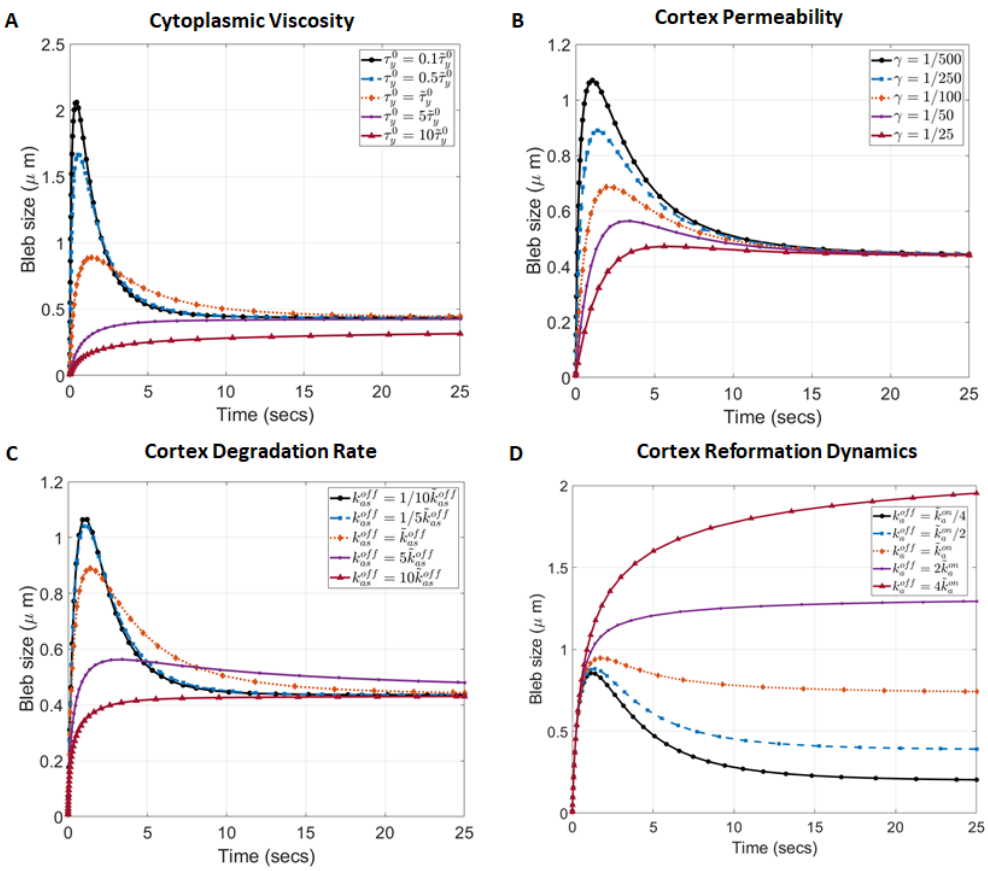


Figure 5: **Influence of viscoelastic properties and actin dynamics on bleb size.** Effect of A) cytoplasmic viscosity B) cortex permeability, modeled as the fraction of actin concentration in the cortex (actin scar) at the onset of blebbing C) degradation rate of actin scar (old cortex), D) ratio of actin polymerization to depolymerization rate at the reforming cortex (bleb cortex), on bleb size. Bleb size is measured as the strain of the cell boundary at a single point. $\tilde{r}$ is the baseline value of parameter $r$ reported in Table 2.

First, we wanted to understand how cortex reformation affects the final bleb size and then explore the effect, if any, that cortex degradation, cytoplasmic viscosity and cortex permeability may have on bleb expansion dynamics. Our results, shown in Fig. 5, suggest that a more viscous cytosol will cause blebs to expand monotonically to their resting size, without retracting (Fig. 5A). As the viscosity of the fluid reduces, blebs have a greater initial expansion before retracting to their equilibrium size. Cortex permeability and degradation rate of the actin scar have a similar effect

on bleb expansion dynamics (Fig. 5B,C). As predicted theoretically, none of these factors alter the equilibrium size of blebs. In support of our equilibrium analysis, we see that varying the dynamics of cortex reformation changes the equilibrium bleb size (Fig. 5D). Interestingly, bleb retraction seems to be regulated by the relative rate of actin polymerization ($k_{ab}^{on}$) and depolymerization ($k_{ab}^{off}$) at the bleb cortex. Particularly, when $k_{ab}^{off} < k_{ab}^{on}$ no retraction occurs and the blebs expand monotonically to an equilibrium size. On the contrary, blebs retract before reaching equilibrium size when $k_{ab}^{off} \geq k_{ab}^{on}$.

## Cell area increases with decreasing linker protein strength

Having validated our 1D model by reproducing known effects of mechanical and viscoelastic parameters on bleb size and bleb expansion dynamics, we sought to test the hypothesis that weakening linker protein strength is sufficient to reduce bleb size. While this is possible with the 1D model, the 2D model provides a more realistic representation of the physics at play during blebbing. Thus, we proceed to validate the 2D model presented in Eqns. (4)-(7).

The bleb expansion dynamics over the first 10 seconds, can be observed in Fig. 6A. we simulated bleb expansion for 10 seconds instead of 25 seconds (done in 1D case) since our prior experiments [2] and 1D simulations (in this work) suggest that blebs achieve close to 90% of the equilibrium size within 10 seconds. This also helped to reduce the total run time for computational experiments without altering the results significantly. Over the first two seconds, the membrane expands freely to a maximum bleb area and then slowly retracts, once cortex reformation and degradation begin. Consistent with our 1D results, increasing the excess pressure $P_{start}$ leads to formation of larger blebs (Fig. 6B). Similarly, increasing membrane stiffness and cortical stiffness both reduce bleb size, with cortical stiffness having a greater effect (Fig. 6 C,D). In agreement with the 1D model, the dynamics of cortex reformation, in particular the ratio of actin polymerization to depolymerization rate, also affects bleb size (Fig. 6D).

We first examined the effect of linker protein strength on the critical area of the cell. This is the cell area when the prevailing intracellular pressure is balanced by the viscoelastic boundary. Observe from Fig. 7A that the critical area increases as the linker stiffness is reduced, with a greater

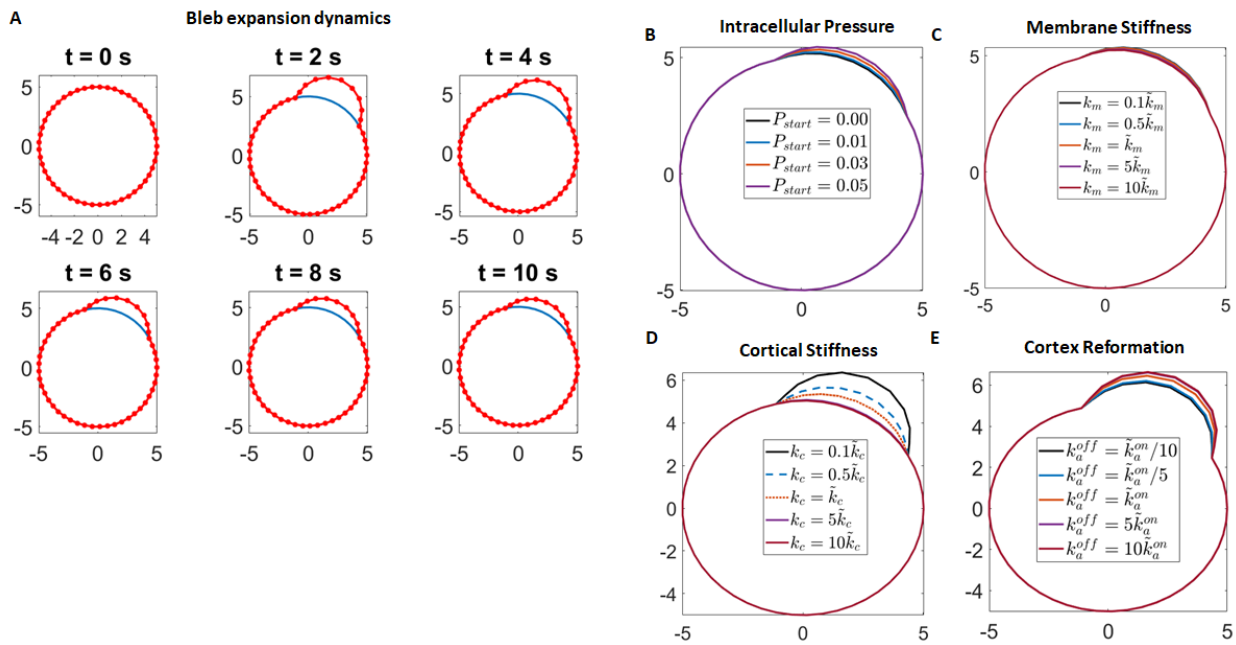


Figure 6: **Validation of 2D blebbing model.** A) Dynamics of bleb expansion for the first 10 seconds after membrane detachment. Effect of B) intracellular pressure C) membrane stiffness D) cortical stiffness and E) cortex reformation on bleb size. $\tilde{r}$ is the baseline value reported in Table 2 of a parameter $r$

critical area for higher intracellular pressure. The difference in critical area between high and low pressure is smaller for stronger linker proteins ($k_a \geq 0.1$) and increases as the linker stiffness is reduced ($k_a < 0.1$). This observation agrees with our experimental results, where we had very little difference between the cell areas of Ax2 *Dictyostelium* cells under high and low agarose but a greater difference between *talA* null cells under similar conditions (Fig. 3D). Note that the range of simulated critical cell area is consistent with the area measured in our experimental data. In particular, the median cell area for Ax2 cells is around 32 $\mu m^2$ whereas that for *talA* null is around 35 $\mu m^2$ ($Fig.$ 3$D$, high confinement).

We also examined the effect that an excess pressure will have on the cell area and boundary displacement, without initiating blebs. This is important since our working hypothesis suggests that cell area increases resulting from reduced linker stiffness limits the driving pressure necessary for bleb expansion. To test this, we run our model for the same time duration (10 seconds), without detaching linker proteins (i.e initiating blebs), for different linker stiffness. Our results,

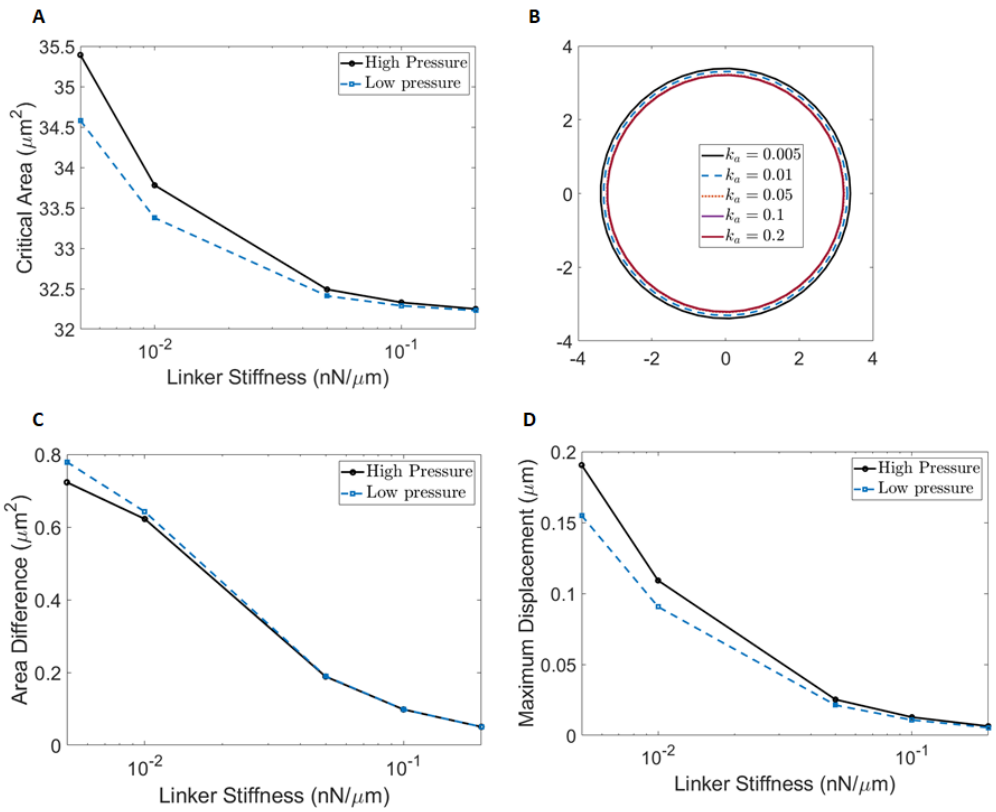


Figure 7: **Response of cell boundary to excess pressure.** Response of cell boundary to excess pressure of $0.05nN/(\mu m^2)$), without detaching linker proteins, under varying linker protein strength over a 10 second duration. No blebs are initiated. A) Critical cell area prior to application of excess pressure. B) Final location of cell boundary after application of excess pressure when resting pressure is $0.08nN/(\mu m^2)$). C) Difference in final area of cell and the critical area under high ($0.08nN/(\mu m^2)$)) and low ($0.06nN/(\mu m^2)$)) resting intracellular pressure. D) Maximal displacement of the cell boundary from its location at critical strain.

shown in Fig. 7B, suggests that under the same intracellular pressure, the cell boundary is pushed out further in response to excess pressure when weaker linker proteins are present. Additionally, the maximum displacement of the cell boundary from its initial configuration is greater for high resting pressure than for lower pressure (Fig. 7D). It is note worthy that the difference between the final cell area (after application of excess pressure and no bleb formation) and the critical cell area (before application of excess pressure) is small relative to the scale of the critical area of the cell (Fig. 7C). Thus, our model does not yield a significant change in cell area in response to excess pressure, when blebs are not initiated.

### Bleb area decreases with decreasing linker protein strength

Next, we allowed blebs to form (by removing linker proteins from a local region of the cell boundary) and compared the final boundary profile (with a bleb) to the final profile without bleb formation (discussed in the previous section) as well as the critical profile (measured prior to the application of excess pressure). Our results in Fig. 8A qualitatively show that smaller blebs form as the stiffness of the linker protein is reduced. Notice that the cell boundary when blebs are not initiated in response to excess pressure (no-bleb boundary, dashed blue line in Fig. 8A) appears to overlay with the boundary when blebs form (bleb boundary, dotted orange line in Fig. 8A) everywhere except at the blebbing region. These two boundaries (bleb and no bleb) also appear to differ more from the critical boundary (solid black line in Fig. 8A) as the linker protein stiffness is decreased. Our simulations thus show that the cell boundary is uniformly pushed out in response to excess pressure everywhere (as shown in Fig. 7b), with a greater extension where linker proteins are detached (yielding blebs). Based, on this observation, we quantified the bleb area formed by subtracting the cell area enclosed by the bleb boundary (dotted orange line in Fig. 8A) from the area enclosed by the no-bleb boundary (dashed blue line in Fig. 8A). We can observe quantitatively that bleb area decreases as linker protein stiffness decreases, with larger blebs formed for higher pressure ( Fig. 8B). Notice that the size of blebs at our baseline value for linker stiffness (0.1nN/$\mu m$) agrees with the median bleb area for wild type cells shown in our experimental data.

## Discussion

Our work investigates the role of TalA and actin dynamics in regulating bleb size and frequency. TalA is known to localize to the posterior of chemotaxing *Dictyostelium* cells and helps to direct blebs to the leading edge of the cell [9, 34]. A recent study suggested that TalA enrichment is inversely proportional to blebbing after observing profusive blebbing in a double mutant (*talA*/*talB* null)[9]. We wanted to test whether this phenotype would be observed in a single deletion of *talA*. We find that *Dictyostelium* cells without TalA rarely bleb. These mutant cells also have a larger surface area and produce significantly smaller blebs compared to wild type cells (Fig. 3). This

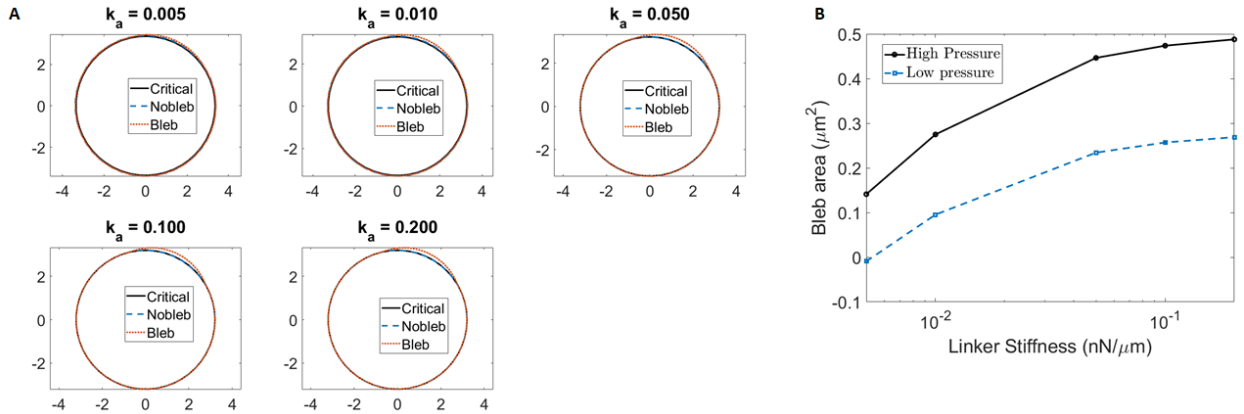


Figure 8: **Effect of linker protein strength on bleb size.** A) Bleb shape at different linker stiffness at high intracellular pressure. 'Critical' boundary (solid black line) is the critical cell boundary which balances the resting intracellular pressure. The 'Nobleb' boundary (dashed blue line) is the displaced boundary after application of excess pressure, without detaching linker proteins locally. The 'Bleb' boundary (dotted orange line) is the final cell boundary when blebs form. B) Bleb area for high and low resting pressure with varying linker stiffness.

result is startling and in direct contrast to the existing school of thought that cells would increase blebbing in response to an absence of TalA [9]. Indeed, one would expect that by removing one of the two known linker proteins in *Dictyostelium*, the attachment of the membrane to the cortex would be significantly reduced, making it easier for blebs to form. Our observations suggest that *talA* null cells have reduced intracellular pressure, which makes it less likely for blebs to form. Thus, in addition to directing blebs to the front of the cell, this study suggests that TalA helps to maintain the intracellular pressure required for bleb formation.

We hypothesize that the pressure reduction in *talA* null cells comes from a uniform extension of the cell membrane away from the cortex, due to the presence of a much weaker attachment of the membrane to the cortex via *talB*. To verify the mechanical viability of this hypothesis, we developed a mathematical model of bleb expansion and examined the effect of weakening the strength of linker proteins on bleb size and cell area. Our model improves upon existing models of bleb expansion by allowing for a dynamic change in the density of linker proteins in response to the prevailing hydrostatic pressure, prior to bleb formation. This framework is needed to capture the cells initial effort to balance any excess pressure by deforming the membrane before linker proteins are detached to form blebs. The model also accounts for the dynamic formation of a

482 cortex beneath the protruded membrane as well as its degradation at the old location of the cortex,
483 with parameters determined from a prior study analyzing blebbing data [2]. Our model also allows
484 for an investigation of the effect of actin dynamics on bleb formation, something that has not been
485 studied mechanistically hitherto.

486 Simulations of our model show that decreasing the linker protein strength indeed decreases bleb
487 size (Fig. 8) and causes a greater uniform outward extension of the cell boundary in non-blebbing
488 regions (Fig. 7B). We reason that the extension of the cell boundary increases the surface area to
489 volume ratio of the cell and consequently decreases the prevailing intracellular pressure. This effect
490 is captured by the volume preserving term in our model for pressure (Eqn. 8). The key outcome of
491 our modeling effort is in the conclusion that the extension of the cell boundary due to weaker linker
492 proteins, though small (Fig. 7B,C), is sufficient to reduce the intracellular pressure and limit bleb
493 size. This conclusion is not obvious from our experimental results and necessitated mathematical
494 modeling.

495 Additionally, our model simulations and equilibrium analysis support the existing view point
496 that bleb size is regulated by membrane and cortical stiffness as well as intracellular pressure
497 [26, 27]. We also observed that blebs expand to a larger size as the ratio of actin polymerization
498 rate to depolymerization increases in the reforming cortex (Fig. 5D, Fig. 6D). Interestingly, we
499 observed that blebs undergo a partial retraction when the polymerization rate is less than or equal
500 to the depolymerization rate and expand monotonically, otherwise. Hitherto, bleb retraction has
501 been soley associated with the contractile activity of myosin [13, 5, 21]. This study suggests that
502 retraction can be driven by actin dynamics without the need to invoke myosin II.

503 Our modeling and experiments suggest that weakening the strength of linker proteins results
504 in a uniform extension of the membrane from the cortex, which limits the driving pressure for
505 bleb formation. Consequently, a double mutant should have a more significant reduction in bleb
506 size (since there will be more pressure relief) and be less likely to make blebs. It is unclear to us
507 why a double deletion of *talA* and *talB* would bleb profusely, as suggested in [9]. One possibility
508 is that these proteins have very different roles in blebbing and as such more experiments need to
509 be done to quantify blebbing in a single *talB* deletion. The experimental data presented in [9] to

support profusive blebbing of the double *talA,talB* mutant shows membrane protrusions without visible cytoplasm. It is unclear if these go through the bleb cycle described in Fig. 2. There is also no quantification of the frequency or size of blebs in comparison to wild type. Thus, it will be informative to conduct new experiments for the double mutant to clarify the role of *talB* in blebbing.

## Author Contributions

**S.H.Dinuka de Silva:** Mathematical modeling and simulation, Formal analysis, Visualization, Writing-original draft. **Emily Movsumova:** Analysis of experimental data, Visualization, Formal analysis, Writing-original draft. **Jessica Reznik:** Analysis of experimental data, Visualization, Formal analysis, Writing-original draft. **Zully Santiago:** Methodology, Investigation. **Derrick Brazill:** Investigation, Conceptualization, Formal analysis. **Emmanuel Asante-Asamani:** Methodology, Formal analysis, Investigation, Conceptualization.

# References


[1] R. Alert and J. Casademunt, Bleb nucleation through membrane peeling, *Physical review letters*, **116** (2016), 068101.

[2] E. Asante-Asamani, M. Dalton, D. Brazill and W. Strychalski, Modeling the dynamics of actin and myosin during bleb stabilization, *Applied Mathematics for Modern Challenges*, URL https://www.aimsciences.org/article/id/65ee9886c26d215a60507378.

[3] E. Asante-Asamani, D. Grange, D. Rawal, Z. Santiago, J. Loustau and D. Brazill, A role for myosin ii clusters and membrane energy in cortex rupture for dictyostelium discoideum, *Plos one*, **17** (2022), e0265380.

[4] H. Blaser, M. Reichman-Fried, I. Castanon, K. Dumstrei, F. L. Marlow, K. Kawakami, L. Solnica-Krezel, C.-P. Heisenberg and E. Raz, Migration of zebrafish primordial germ cells: a role for myosin contraction and cytoplasmic flow, *Developmental cell*, **11** (2006), 613–627.

[5] G. Charras and E. Paluch, Blebs lead the way: how to migrate without lamellipodia, *Nature reviews Molecular cell biology*, **9** (2008), 730–736.

[6] G. T. Charras, M. Coughlin, T. J. Mitchison and L. Mahadevan, Life and times of a cellular bleb, *Biophysical journal*, **94** (2008), 1836–1853.

[7] G. T. Charras, J. C. Yarrow, M. A. Horton, L. Mahadevan and T. Mitchison, Non-equilibration of hydrostatic pressure in blebbing cells, *Nature*, **435** (2005), 365–369.

[8] C. Choi, H. Patel and D. Barber, Expression of actin-interacting protein 1 suppresses impaired chemotaxis of *Dictyostelium* cells lacking the $na^+$ $h^+$ exchanger nhe1.

[9] S. Collier, P. Paschke, R. R. Kay and T. Bretschneider, Image based modeling of bleb site selection, *Scientific reports*, **7** (2017), 6692.

[10] H. B. da Rocha, J. Bleyer and H. Turlier, A viscous active shell theory of the cell cortex, *Journal of the Mechanics and Physics of Solids*, **164** (2022), 104876.

[11] O. T. Fackler and R. Grosse, Cell motility through plasma membrane blebbing, *The Journal of cell biology*, **181** (2008), 879–884.

[12] P. Friedl and K. Wolf, Tumour-cell invasion and migration: diversity and escape mechanisms, *Nature reviews cancer*, **3** (2003), 362–374.

[13] M. Fritzsche, R. Thorogate and G. Charras, Quantitative analysis of ezrin turnover dynamics in the actin cortex, *Biophys. J.*, **106** (2014), 343–353.

[14] J. M. García-Arcos, A. Jha, C. M. Waterman and M. Piel, Blebology: principles of bleb-based migration, *Trends in Cell Biology*.

[15] A. Guzman, R. C. Avard, A. J. Devanny, O. S. Kweon and L. J. Kaufman, Delineating the role of membrane blebs in a hybrid mode of cancer cell invasion in three-dimensional environments, *Journal of cell science*, **133** (2020), jcs236778.

[16] M. Ibo, V. Srivastava, D. N. Robinson and Z. R. Gagnon, Cell blebbing in confined microfluidic environments, *PLoS One*, **11** (2016), e0163866.

[17] M. A. Khajah and Y. A. Luqmani, Involvement of membrane blebbing in immunological disorders and cancer, *Medical Principles and Practice*, **25** (2016), 18–27.

[18] N. Khalilgharibi, J. Fouchard, N. Asadipour, R. Barrientos, M. Duda, A. Bonfanti, A. Yonis, A. Harris, P. Mosaffa, Y. Fujita et al., Stress relaxation in epithelial monolayers is controlled by the actomyosin cortex, *Nature physics*, **15** (2019), 839–847.

[19] C. T. Mierke, Physical view on migration modes, *Cell Adhesion & Migration*, **9** (2015), 367–379.

[20] J. Niewöhner, I. Weber, M. Maniak, A. Müller-Taubenberger and G. Gerisch, Talin-null cells of dictyostelium are strongly defective in adhesion to particle and substrate surfaces and slightly impaired in cytokinesis, *The Journal of cell biology*, **138** (1997), 349–361.

[21] E. K. Paluch and E. Raz, The role and regulation of blebs in cell migration, *Current opinion in cell biology*, **25** (2013), 582–590.

[22] E. Raz, Guidance of primordial germ cell migration, *Current opinion in cell biology*, **16** (2004), 169–173.

[23] Z. Santiago, *Towards a Mathematical Model of Motility Using Dictyostelium discoideum: Proteins and Geometric Features that Regulate Bleb-Based Motility*, PhD thesis, City University of New York, 2019.

[24] Z. Santiago, J. Loustau, D. Meretzky, D. Rawal and D. Brazill, Advances in geometric techniques for analyzing blebbing in chemotaxing dictyostelium cells, *Plos one*, **14** (2019), e0211975.

[25] S. Strömblad, Cancer biology: Hypoxia-induced talin tail-docking sparks cancer metastasis, *Current Biology*, **32** (2022), R79–R81.

[26] W. Strychalski and R. D. Guy, A computational model of bleb formation, *Mathematical medicine and biology: a journal of the IMA*, **30** (2013), 115–130.

[27] J.-Y. Tinevez, U. Schulze, G. Salbreux, J. Roensch, J.-F. Joanny and E. Paluch, Role of cortical tension in bleb growth, *Proceedings of the National Academy of Sciences*, **106** (2009), 18581–18586.

[28] J.-Y. Tinevez, U. Schulze, G. Salbreux, J. Roensch, J.-F. Joanny and E. Paluch, Role of cortical tension in bleb growth, *Proc. Natl. Acad. Sci. USA*, **106** (2009), 18581–18586.

[29] M. Tozluoğlu, A. L. Tournier, R. P. Jenkins, S. Hooper, P. A. Bates and E. Sahai, Matrix geometry determines optimal cancer cell migration strategy and modulates response to interventions, *Nature cell biology*, **15** (2013), 751–762.

[30] M. Tsujioka, L. Machesky, S. Cole, K. Yahata and K. Inouye, A unique talin homologue with a villin headpiece-like domain is required for multicellular morphogenesis in dictyostelium, *Current Biology*, **9** (1999), 389–394.

[31] M. Tsujioka, Cell migration in multicellular environments, *Development, growth & differentiation*, **53** (2011), 528–537.

[32] M. Tsujioka, T. Q. Uyeda, Y. Iwadate, H. Patel, K. Shibata, T. Yumoto and S. Yonemura, Actin-binding domains mediate the distinct distribution of two dictyostelium talins through different affinities to specific subsets of actin filaments during directed cell migration, *Plos one*, **14** (2019), e0214736.

[33] M. Tsujioka, K. Yoshida and K. Inouye, Talin b is required for force transmission in morphogenesis of dictyostelium, *The EMBO journal*, **23** (2004), 2216–2225.

[34] M. Tsujioka, S. Yumura, K. Inouye, H. Patel, M. Ueda and S. Yonemura, Talin couples the actomyosin cortex to the plasma membrane during rear retraction and cytokinesis, *Proceedings of the National Academy of Sciences*, **109** (2012), 12992–12997.

[35] L. Yang, J. C. Effler, B. L. Kutscher, S. E. Sullivan, D. N. Robinson and P. A. Iglesias, Modeling cellular deformations using the level set formalism, *BMC systems biology*, **2** (2008), 1–16.

[36] K. Yoshida and T. Soldati, Dissection of amoeboid movement into two mechanically distinct modes, *Journal of cell science*, **119** (2006), 3833–3844.

[37] E. Zatulovskiy, R. Tyson, T. Bretschneider and R. R. Kay, Bleb-driven chemotaxis of dictyostelium cells, *Journal of Cell Biology*, **204** (2014), 1027–1044.